# Shishiodoshi unidirectional energy transfer mechanism in phenylene ethynylene dendrimers

S. Fernandez-Alberti,[1,a)] Adrian E. Roitberg,[2] Valeria D. Kleiman,[3] T. Nelson,[4] and S. Tretiak[4]

[1]*Universidad Nacional de Quilmes, Roque Saenz Peña 352, B1876BXD Bernal, Argentina*
[2]*Quantum Theory Project, Department of Chemistry, University of Florida, Gainesville, Florida 32611, USA*
[3]*Department of Chemistry, University of Florida, Gainesville, Florida 32611, USA*
[4]*Theoretical Division, Center for Nonlinear Studies (CNLS), and Center for Integrated Nanotechnologies (CINT), Los Alamos National Laboratory, Los Alamos, New Mexico 87545, USA*

Non-adiabatic excited-state molecular dynamics is used to study the ultrafast intramolecular energy transfer between two-, three-, and four-ring linear polyphenylene ethynylene chromophore units linked through meta-substitutions. Twenty excited-state electronic energies, with their corresponding gradients and nonadiabatic coupling vectors were included in the simulations. The initial laser excitation creates an exciton delocalized between the different absorbing two-ring linear PPE units. Thereafter, we observe an ultrafast directional change in the spatial localization of the transient electronic transition density. The analysis of the intramolecular flux of the transition density shows a sequential through-bond two-ring→three-ring→four-ring transfer as well as an effective through-space direct two-to-four ring transfer. The vibrational excitations of C≡C stretching motions change according to that. Finally, a mechanism of unidirectional energy transfer is presented based on the variation of the energy gaps between consecutive electronic excited states in response to the intramolecular flux of the transition density. The mechanism resembles a Shishiodoshi Japanese bamboo water fountain where, once the electronic population has been transferred to the state directly below in energy, the two states decouple thereby preventing energy transfer in the opposite direction. © *2012 American Institute of Physics.* [http://dx.doi.org/10.1063/1.4745835]

## I. INTRODUCTION

Understanding the complex electronic dynamics in nano-materials is a critical step for a broad range of technological applications.[1–3] The highly polarizable and delocalized $\pi$-electron manifold of organic conjugated molecules is responsible for many of the unique electronic and photophysical properties associated with these materials.[4] In recent years, many of these materials have become popular candidates for photovoltaic applications, and have lead to new designs for photovoltaic cells. In particular, dendrimers exhibit exceptional light-harvesting capabilities over a broad region of the solar spectrum, and the branched conjugated structure of these macromolecules allow for very efficient energy funneling.[5,6] Developing a clear picture of the photoexcitation dynamics in such materials is essential to providing an accurate description of the underlying photophysical processes such as exciton formation, evolution, and decay via non-adiabatic (NA) dynamics.

The family of dendrimers comprised of polyphenylene ethynylene (PPE) units offers an intriguing system to study because they exhibit both the collection and energy transfer processes that are of interest in photosynthetic systems.[7–9] Their highly efficient intramolecular energy transfer has been the subject of several theoretical and experimental studies.[7,10,8,9,13,15,17] The perylene-terminated dendrimer called the nanostar is among the most studied compounds.[11,16,17,13] This molecule exhibits a regular structure possessing numerous peripheral groups, branched repeat units, and a perylene core. The peripheral groups are composed of two-ring linear PPE segments, and the branched repeat units are built from linear PPE segments whose lengths increase from the periphery to the core. The linear PPE segments are linked by meta-substitutions at the branching phenylene nodes. These meta-branchings localize excitons within each linear PPE fragment hindering any further delocalization of electrons across the dendrimer framework.[13,12] In this way, the linear PPE fragments act as weakly coupled chromophore units[13,14] allowing the total absorption spectrum to be interpreted as the sum of their contributions.[15–17] The difference in length of the linear PPE fragments creates an intramolecular energy gradient from the periphery to the core. When the peripheral two-ring chromophores are initially excited, the energy is transferred non-radiatively down the branches to the core with nearly 100%.

The concerted electronic and vibrational energy transfer has been previously demonstrated in the model dendrimer composed of meta-linked two- and three-ring linear PPE units.[18] However, the situation becomes more complicated when additional units and branching sites are included in the system. On one hand, the increased number of intermediate

---
a)Author to whom correspondence should be addressed. Electronic mail: sfalberti@gmail.com.

electronic excited states involved in the process makes it quite difficult to identify them as they evolve with time. The different adiabatic electronic states may mix and cross when their time-dependent energies become close enough. Consequently during the ultrafast energy-transfer process, the energy order criterion to identify the electronic states does not work. Therefore, instead of the common analysis of the average populations of the different electronic states as a function of time, a simplified description of the process is required. In this work we propose the use of the time-dependent localization of the transition density to describe the process. The resulting mechanism for the energy-transfer process should be consistent with this picture regardless the notation used to classify the individual electronic excited states. On the other hand, the unidirectional energy transferin more complex molecule may be via several distinct pathways with different efficiencies. More precisely, through-space and sequential through-bond energy transfer mechanisms are expected to exist simultaneously and in competition with one another.

A variety of fundamental photophysical processes such as charge and energy transfer are attributed to non-adiabatic (NA) dynamics.[19–24] Molecular dynamics with quantum transitions (MDQT) (Ref. [25]) is a well tested and computationally feasible method to study non-adiabatic molecular dynamics (NA-MD) simulations.[26–32] It enables a separate treatment of electronic (quantum) and nuclear (classical) subsystems. At any given time, the nuclei evolve on a potential energy surface (PES) defined by a single electronic state. Based on Tully's stochastic fewest-switches surface hopping (FSSH) algorithm, the system is able to transition, or hop, at any time during dynamics from the current electronic state to other states according to transition probabilities that are governed by the strengths of the non-adiabatic couplings.

In this study we investigate the ultrafast intramolecular energy transfer between two-, three-, and four-ring linear polyphenylene ethynylene (PPE) chromophore units. This PPE system serves as a model system, similar to the well known "nanostar" dendrimer,[33,34,17] in which directional energy transfer mechanisms can be studied. The molecule is large enough to allow us to address several aspects that were not present in previously studied models. We present a simplified picture of the intramolecular energy transfer process based on the time evolution of the localization of the electronic transition density. Using it, the contributions of the different energy transfer pathways to the energy transfer process are discussed, and a general mechanism is proposed.

We make use of our previously developed non-adiabatic excited state molecular dynamics (NA-ESMD) framework and implement our recently developed state reassignment algorithm[35] to correctly treat trivial unavoided crossings between the numerous coupled electronic states within the surface hopping methodology. Both the through-bond two-ring→three-ring→four-ring transfer pathway and the through-space direct two-ring→four-ring transfer pathway are investigated. An analysis based on the variation of the energy gaps between consecutive electronic excited states in response to the intramolecular flux of the transition density

is presented. We also demonstrate that the vibrational excitations of the C≡C stretching motions change according to the through-bond or through-space mechanism.

## II. METHODS

### A. NA-ESMD background

Within the NA-ESMD framework,[36–38] *direct* nonadiabatic molecular dynamics simulations[39] can be applied to describe photoinduced dynamics in large organic conjugated molecules involving multiple coupled electronic excited states. Such NA-ESMD simulations are performed by combining the molecular dynamics with quantum transitions[40,25,41] (MDQT) approach with "on the fly" analytical calculations of excited state energies,[42–44] gradients[36,45,46] and non-adiabatic coupling[36,47–49] terms. This is possible using the collective electron oscillator (CEO) method[7,50–52] applied at the AM1 (Ref. [53]) semiempirical level in combination with the configuration interaction singles (CIS) formalism to describe correlated excited states. A detailed discussion about the NA-ESMD implementation, advantages, and testing parameters can be found elsewhere.[36,54]

### B. Transition density localization

The CEO approach[55,56] has been used to calculate transition density matrices ($(\rho^{g\alpha})_{nm} \equiv \langle \boldsymbol{\phi}_\alpha(\boldsymbol{r};\boldsymbol{R}(t)) \times |c_m^+ c_n| \boldsymbol{\phi}_g(\boldsymbol{r};\boldsymbol{R}(t))\rangle$) (denoted *electronic normal modes*) using the ground-state density matrix being $\boldsymbol{\phi}_\alpha(\boldsymbol{r};\boldsymbol{R}(t))$ and $\boldsymbol{\phi}_g(\boldsymbol{r};\boldsymbol{R}(t))$ the CIS adiabatic functions of the excited and ground state respectively. $c_m^+ (c_n)$ is creation (annihilation) operator; and $n$ and $m$ refer to atomic orbital (AO) basis functions. Therefore, the net change in the distribution of the electronic density induced by optical excitation from the ground state $g$ to an excited electronic $\alpha$ state can be follow through the diagonal elements of $(\rho^{g\alpha})_{nn}$.[14] At the CIS approximation, the normalization condition $\sum_{n,m} (\rho^{g\alpha})_{nm}^2 = 1$[44,36] is fulfilled. In order to obtain the fraction of the transition density localized on each linear PPE unit (i.e., two-ring, three-ring, and four-ring linear PPE units), we sum up the atomic contributions belonging to each of them as

$$(\rho^{g\alpha})_{X\text{-ring}}^2 = \sum_{n_A m_A} (\rho^{g\alpha})_{n_A m_A}^2 + \left( \sum_{n_A m_B} (\rho^{g\alpha})_{n_A m_B}^2 + \sum_{n_B m_A} (\rho^{g\alpha})_{n_B m_A}^2 \right) + \frac{1}{2} \sum_{n_B m_B} (\rho^{g\alpha})_{n_B m_B}^2, \quad (1)$$

where the index A runs over all atoms localized in the X-ring (X = 2,3,4) linear PPE unit, and the index B runs over atoms localized in between these units. Consequently, in our case $\sum_X (\rho^{g\alpha})_{X\text{-ring}}^2 \approx 1$ since meta-conjugation blocks long-range electronic interactions.

### C. Molecular dynamics simulations

NA-ESMD simulations of the photoexcitation and intramolecular energy transfer between *m*-branched PPE units were performed on the model molecule depicted in
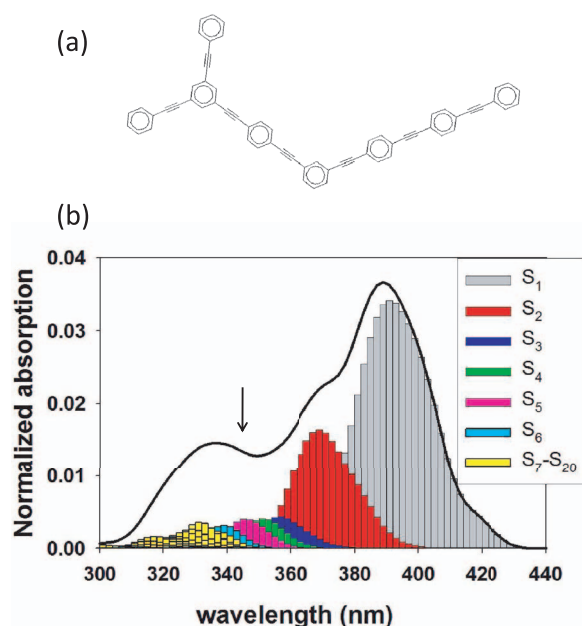
(a)



(b)



FIG. 1. (a) Chemical structure of the molecule studied in this work. A pair of two-ring units, a three-ring, and four-ring linear poly(phenylene ehynylene) units linked by meta-substitution. (b) Simulated absorption spectrum (solid line). Contributions of the different excited states are also depicted. The arrow indicates the maximum of the laser excitation wavelength used in the simulations.

Figure 1(a). To describe the motion of the classically treated nuclei, the Langevin equation at constant temperature[57] with a friction coefficient $\gamma$ of 2.0 ps$^{-1}$ was used.[58] This value has been chosen to allow an efficient temperature coupling.[57] As it has been previously shown, larger values of $\gamma$ lead to faster vibrational relaxation. The resulting vibrational damping reduces the value of the computed nonadiabatic coupling terms (NACTs) (Refs. 54 and 59) with the concomitant effects on the electronic relaxation. Nevertheless, only dramatic changes (at least an order of magnitude) in the $\gamma$ value seem to lead to any significant effects in the overall relaxation rates.[54]

The initial positions and momenta for the NA-ESMD were taken from a previously equilibrated 500 ps of MD simulations at 300 K with the molecule in the ground electronic state and a classical time step $\Delta t = 0.5$ fs. The initial excited state was chosen according to a Frank-Condon window defined as

$$g_\alpha(\boldsymbol{r}, \boldsymbol{R}) = \exp\left[-T^2(E_{laser} - \Omega_\alpha)^2\right], \quad (2)$$

where $E_{laser}$, expressed in units of fs$^{-1}$ as well as $\Omega_\alpha$, represents the energy of a laser centred at 346 nm that corresponds to the maximum wavelength of the sum of the contributions of states S$_n$ ($n \geq 3$) to the theoretical absorption spectrum (see Figure 1(b)). The laser shape is assumed to be a Gaussian $f(t)$ = exp ( − $t^2/2T^2$), T$^2$ = 42.5 fs, that corresponds to a Gaussian FWHM of 100 fs. Thus, the initial excited state is selected according to the relative values of the $g_\alpha(\boldsymbol{r}, \boldsymbol{R})$ weighted by the oscillator strengths of each state $\alpha$.

For all simulations, the AM1/CIS level of theory has been used. Twenty excited electronic states and their nonadiabatic coupling vectors $\boldsymbol{d}_{\alpha\beta}$ were included in the simulations. Details about our NA-ESMD implementation and parameters can be

found elsewhere.[54] A swarm of 400 NA-ESMD trajectories were propagated for 150 fs at 300 K. The nuclei are propagated with the velocity Verlet integration method[60] with a classical time step $\Delta t = 0.1$ fs. The differential equations for the propagation in time of the electronic quantum coefficients are solved using Runge-Kutta-Verner fifth- and sixth-order method as implemented in the NA-ESMD framework[36] using a quantum time step $\delta t = \Delta t/4$.

## III. RESULTS AND DISCUSSION

NA-ESMD simulations have been performed in order to study the ultrafast intramolecular energy transfer that takes place in the model branched dendritic molecule, depicted in Figure 1(a), following photoexcitation. The initial excited states are populated according to their contributions to the simulated absorption spectrum shown in Figure 1(b) using a Frank-Condon window defined by a Gaussian shaped laser centered at 346 nm with FWHM of 100 fs. According to experimental spectroscopic results, the different excited states are initially localized in the different linear PPE units.[13] In Figure 2 we show the initial localization of the electronic transition density for the four lowest excited states. As can be seen, the lowest singlet S$_1$ state is mainly localized in the 4-ring linear PPE unit, the subsequent state in the energy-order, the S$_2$ state, is mainly localized in the 3-ring linear PPE unit, and the higher energy S$_3$ and S$_4$ states are partially delocalized in the 2-ring linear PPE units. Therefore, we confirm that the dendrimer molecule can be effectively represented as an ensemble of weakly coupled linear PPE chromophore units. In agreement with previous works on related systems,[51,52,61,62] the absorption spectra can be analyzed as the sum of the absorption of each separate linear PPE photoactive unit: two-ring, three-ring, and four-ring linear PPE units. That is, according to the contributions of the different excited states to the total absorption spectra shown in Figure 1(b), the peak at 390 nm corresponds to the absorption of the S$_1$ state whose transition density is mainly localized in the four-ring unit, the shoulder at 370 nm corresponds to S$_2$ with the transition density mainly localized in the three-ring unit, and the peak at 336 nm represents a superposition of states mainly localized in the two-ring unit and higher frequency states localized on different bonds of the molecule. A detailed analysis of the states that contribute to the latter peak has shown that states mainly localized in the two-ring units
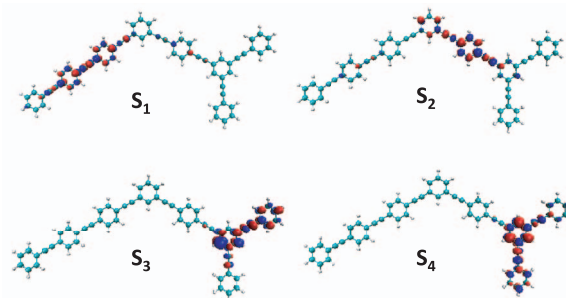


FIG. 2. Initial localization of the electronic transition densities for the four lowest excited states.
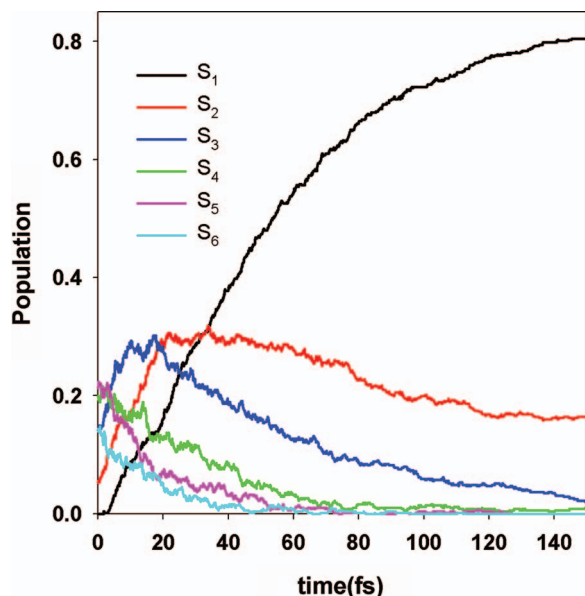
FIG. 3. Population on each electronic surface as a function of time obtained from the fraction of trajectories in each state.
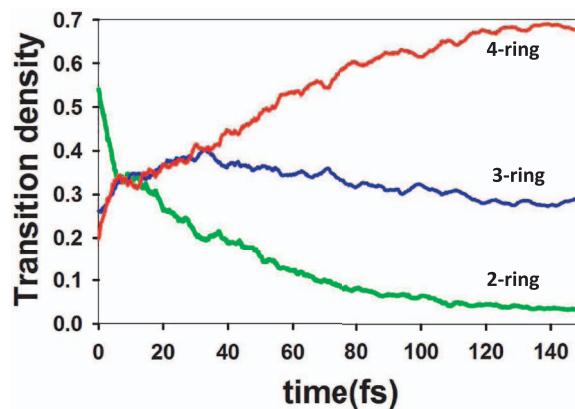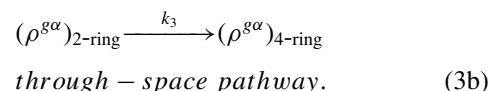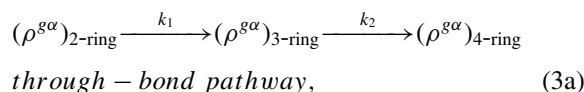


FIG. 4. Time-dependent average of the fraction of the transition density localized in the two- (green), three- (blue), and four-ring (red) linear PE units.

correspond to states in the range [$S_3$:$S_6$] presenting a joint maximum absorption at 346 nm. Therefore, the excitation at 346 nm allows us to maximize the initial localization of the electronic transition density on the two-ring units.

The time evolution of the populations on each electronic excited state after photoexcitation is shown in Figure 3. While 20 excited states have been considered during the NA-ESMD simulations, for the sake of simplicity only the sixth lowest states are displayed. States relevant to the intramolecular energy transfer process can be classified into three categories.[58] On one hand, we have the $S_4$-$S_6$ states that lose their initial populations in about 80 fs. These states show transition densities mainly localized in the two-ring units. On the other hand, $S_2$ and $S_3$ states actually act as intermediate states increasing their populations during the first 20 fs and subsequently depleting but at slower rates. These states are localized either in the two-ring and three-ring ring units since geometrical distortions can affect the energy order of their corresponding diabatic states throughout the photoinduced dynamics. Finally, the $S_1$ state, mainly localized in the four-ring unit, increases its population throughout the entire simulation reaching a final value of ~80%.

The large number of intermediate electronic excited states involved in the process makes it quite difficult to identify them as they evolve with time. For the sake of simplicity, the unidirectional energy transfer can be revealed by following the changes in the localization of the electronic transition density of the current state instead of the confusing adiabatic time evolution of the electronic populations. That is, the simple identification of the electronic excited states by energy ordering is not useful in this respect due to the multiple crossings and mixing that the adiabatic states undergo over time. In Figure 4 the time-dependent average of the fraction of the transition density localized in the two-, three-, and four-ring linear PPE units (($\rho^{g\alpha}$)$^2_{X\text{-ring}}$, with X = 2,3, and 4 calculated using Eq. (1)) is shown. As can be seen, initially the transition

density is mainly localized in the two-ring unit but an almost complete ultrafast electronic energy transfer to the three- and four-ring linear PPE units takes place in ~80–100 fs. Furthermore, a transient increase in the localization of the transition density in the three-ring unit indicates that this linear chromophore unit acts as a bridge connecting the two- and four-ring units. Finally, as a result of the electronic energy flux throughout the molecule, the average transition density becomes more and more localized in the four-ring unit. Based on our data, we postulate a kinetic scheme of the following type:

$$(\rho^{g\alpha})_{2\text{-ring}} \xrightarrow{k_1} (\rho^{g\alpha})_{3\text{-ring}} \xrightarrow{k_2} (\rho^{g\alpha})_{4\text{-ring}}$$
$$through-bond\ pathway, \qquad (3a)$$

$$(\rho^{g\alpha})_{2\text{-ring}} \xrightarrow{k_3} (\rho^{g\alpha})_{4\text{-ring}}$$
$$through-space\ pathway. \qquad (3b)$$

By fitting the evolution in time of $(\rho^{g\alpha})_{X\text{-ring}}$ with (X = 2,3,4) (see Figure 4), we obtain values of $k_1 = 0.009$ fs$^{-1}$ ($\tau_1 = 1/k_1 = 111$ fs), $k_2 = 0.003$ fs$^{-1}$ ($\tau_2 = 1/k_2 = 333$ fs), and $k_3 = 0.005$ fs$^{-1}$ ($\tau_2 = 1/k_2 = 200$ fs).

Let us next analyze the intramolecular energy transfer pathways involving the participation of the different linear PPE units of the system. The unidirectional energy transfer from two to four rings can occur through two distinct channels, (a) the through-space direct pathway two-ring→four-ring (Eq. (3a)), and (b) the through-bond sequential transfer two-ring→three-ring → four-ring (Eq. (3b)). Our goal is to distinguish between these two possible pathways and to analyze the contribution of each of them to the final unidirectional energy transfer. Taking into account that the changes in the fraction of transition density localized in each linear PPE unit during the *i*th classical time step $\Delta t$ of the *j*th trajectory satisfies

$$\sum_X \Delta_i \left(\rho^{g\alpha}_j\right)^2_{X\text{-ring}} = 0, \quad (X = 2, 3, 4) \qquad (4)$$

with

$$\Delta_i \left(\rho^{g\alpha}_j\right)^2_{X\text{-ring}} = \Delta_i \left(\rho^{g\alpha}_j\right)^2_{X\text{-ring}\to Y\text{-ring}} + \Delta_i \left(\rho^{g\alpha}_j\right)^2_{X\text{-ring}\to Z\text{-ring}}$$

(X, Y, Z = 2, 3, 4 alternatively).

It is straightforward to obtain the *effective* energy transfers $\Delta_i(\rho_j^{g\alpha})^2_{\text{X-ring}\rightarrow\text{Y-ring}}$ and $\Delta_i(\rho_j^{g\alpha})^2_{\text{X-ring}\rightarrow\text{Z-ring}}$ considering the minimum possible path between them. On one hand, for the generic cases where effective X-ring → Y-ring + Z-ring transfers are observed (i.e., $\Delta_i(\rho_j^{g\alpha})^2_{\text{X-ring}} < 0$, while $\Delta_i(\rho_j^{g\alpha})^2_{\text{Y-ring}}$ and $\Delta_i(\rho_j^{g\alpha})^2_{\text{Z-ring}}$ are $> 0$), we consider that the *net gain* of transition densities in the Y-ring and Z-ring PPE units comes through the direct transfer from the X-ring PPE unit, subsequently

$$\Delta_i(\rho_j^{g\alpha})^2_{\text{X-ring}\rightarrow\text{Y-ring}} = -\Delta_i(\rho_j^{g\alpha})^2_{\text{Y-ring}},$$
$$\Delta_i(\rho_j^{g\alpha})^2_{\text{X-ring}\rightarrow\text{Z-ring}} = -\Delta_i(\rho_j^{g\alpha})^2_{\text{Z-ring}}. \tag{5}$$

On the other hand, for the generic cases where effective X-ring + Y-ring → Z-ring transfers are observed (i.e., $\Delta_i(\rho_j^{g\alpha})^2_{\text{X-ring}}$, and $\Delta_i(\rho_j^{g\alpha})^2_{\text{Y-ring}}$ are $< 0$ while $\Delta_i(\rho_j^{g\alpha})^2_{\text{Z-ring}}$ is $> 0$), no transfer between X- and Y-ring PPE units is considered, and

$$\Delta_i(\rho_j^{g\alpha})^2_{\text{X-ring}\rightarrow\text{Z-ring}} = -\Delta_i(\rho_j^{g\alpha})^2_{\text{X-ring}},$$
$$\Delta_i(\rho_j^{g\alpha})^2_{\text{Y-ring}\rightarrow\text{Z-ring}} = -\Delta_i(\rho_j^{g\alpha})^2_{\text{Y-ring}}. \tag{6}$$

Figure 5(a) shows the average cumulative time-dependent change of the transition density localized in the four-ring linear PPE unit calculated as

$$\Delta(\rho^{g\alpha})^2_{4\text{-ring}}(t) = \Delta(\rho^{g\alpha})^2_{2\text{-ring}\rightarrow 4\text{-ring}}(t)$$
$$+ \Delta(\rho^{g\alpha})^2_{3\text{-ring}\rightarrow 4\text{-ring}}(t) \tag{7}$$

being $\Delta(\rho^{g\alpha})^2_{2\text{-ring}\rightarrow 4\text{-ring}}(t)$ and $\Delta(\rho^{g\alpha})^2_{3\text{-ring}\rightarrow 4\text{-ring}}(t)$ the average *effective* two-to-four ring and three-to-four ring transfers, respectively,

$$(\rho^{g\alpha})^2_{2\text{-ring}\rightarrow 4\text{-ring}}(t) = \frac{1}{M}\sum_{j=1}^{M}\sum_{i=1}^{N_i}\Delta_i(\rho_j^{g\alpha})^2_{2\text{-ring}\rightarrow 4\text{-ring}},$$

$$through-bond\ pathway, \tag{8a}$$

$$(\rho^{g\alpha})^2_{3\text{-ring}\rightarrow 4\text{-ring}}(t) = \frac{1}{M}\sum_{j=1}^{M}\sum_{i=1}^{N_i}\Delta_i(\rho_j^{g\alpha})^2_{3\text{-ring}\rightarrow 4\text{-ring}},$$

$$through-space\ pathway, \tag{8b}$$

with $N_i = \frac{t}{\Delta t}$, M being the total number of trajectories. During the first 150 fs after photoexcitation, 56% of the energy received by the four-ring linear PE unit comes from the direct through-space pathway two-ring→four-ring, while 44% comes from the through-bond sequential transfer two-ring →three-ring →four-ring. As can be seen, the two-ring→four-ring pathway dominates during the very early times of the photoinduced dynamics, that is, at times shorter than 10 fs, after which its rate of energy transfer decreases significantly. On the other hand, the two-ring →three-ring →four-ring pathway seems to present a delay time of ∼ 40 fs until it starts to contribute significantly to $\Delta(\rho^{g\alpha})^2_{4\text{-ring}}$. In the same way, Figure 5(b) represents the average cumulative change of the transition density initially localized in the two-ring linear PPE unit, $\Delta(\rho^{g\alpha})^2_{2\text{-ring}}(t)$, as a result of effective two-to-four ring transfers, $(\rho^{g\alpha})^2_{2\text{-ring}\rightarrow 4\text{-ring}}(t)$, and two-to-three transfers, $(\rho^{g\alpha})^2_{2\text{-ring}\rightarrow 3\text{-ring}}(t)$.
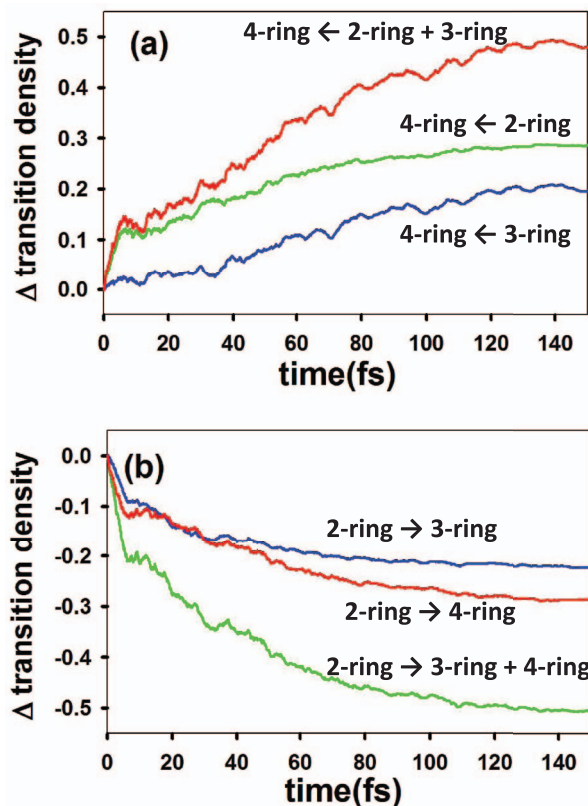


FIG. 5. (a) Average cumulative change of the transition density localized in the four-ring linear PE unit as a result of an effective two-to-four ring transfer (green line), three-to-four ring transfer (blue line), and the sum of the contribution from both channels (red line); (b) Average cumulative change of the transition density initially localized in the two-ring linear PE unit as a result of an effective two-to-four ring transfer (red line), three-to-four ring transfer (blue line), and the sum of the contribution from both channels (green line).

As it has been previously pointed out, the initial state is mainly localized on the two-ring units. Therefore, it is interesting to analyze whether the initial state is localized in only one of the two-ring linear PPE units or if it is spread between both of them. In order to answer this question, we have analyzed the distribution of the initial transition densities (t = 0) localized in the two-ring linear PPE units. As a result, we observe that the initial state is never localized in just one of the two-ring units;[63] instead, the most probable distribution is ∼ 80% in one unit and 20% in the other (see states $S_3$ and $S_4$ in Figure 2). Furthermore, initial states with half of their transition densities localized in each of the two-ring units are also frequent. Our previous studies of simplified molecular models, have revealed the main role the ethynylene triple bonds play in the unidirectional energy transfer process.[18,58] Therefore, it is instructive to evaluate the delocalization of the initial excited state between both two-ring PPE units using the average triple bonds participation number,[64,65] $P_{\text{C}\equiv\text{C}}$, for the transition density of the initial electronic state defined as

$$P_{\text{C}\equiv\text{C}} = \frac{1}{M}\sum_{j=1}^{M}\left[\sum_{i}^{N_{\text{C}\equiv\text{C}}}\left(\sum_{\text{A}\in i}^{N_{\text{AO}}}(\bar{\rho}_j^{g\alpha})^2_{\text{A}}\right)^2\right]^{-1}, \tag{9}$$
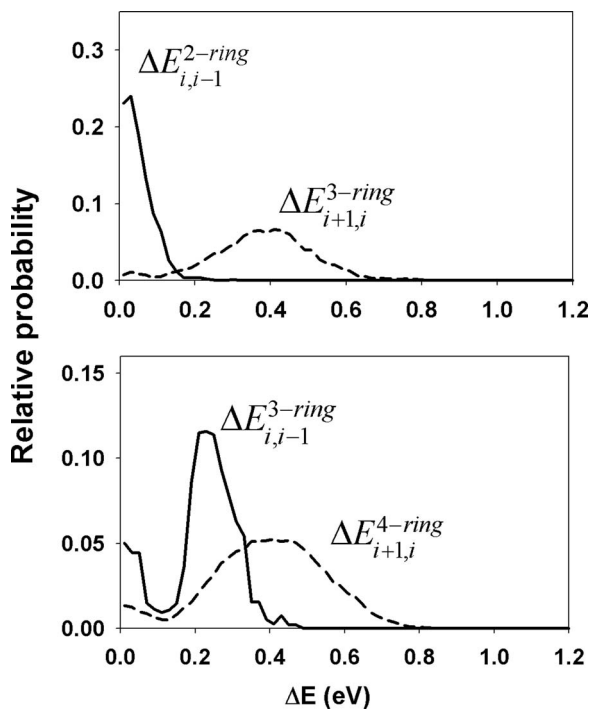
FIG. 6. Histograms of the energy gap $\Delta E_{i,i-1}^{\text{X-ring}}$ between the $S_i$ and $S_{i-1}$ states (solid lines) and the energy gap $\Delta E_{i+1,i}^{\text{X-ring}}$ between the $S_{i+1}$ and $S_i$ states (dashed lines) while nuclei are moving on the $i$ state whose transition density is more than 90% localized in the X-ring linear PE unit (X = 2, 3, and 4).
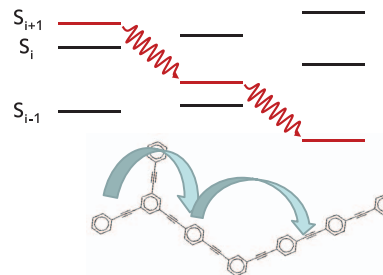


FIG. 7. Jablonski diagram for the Shishiodoshi unidirectional energy transfer mechanism that takes place during the NA-ESMD simulations of the model branched dendritic molecule.

where $N_{C\equiv C} = 7$ is the total number of ethynylene bonds ($C\equiv C$) of the molecule, and the index A runs over the $N_{AO}$ atomic orbitals associated with C atoms of the *ith* triple bond. $\bar{\rho}_j^{g\alpha}$ implies the renormalization of $\rho_j^{g\alpha}$ restricting its calculation to C atoms that belong to triple bonds. In this way, the initial states without significant contributions of the stretching motions in the direction of the ethynylene bonds ($C\equiv C$), (which do not directly participate in the unidirectional energy transfer[58]), are excluded. The initial expected $P_{C\equiv C}$ value should be 1 if the initial state is localized in only one of the two-ring units, and 2 if it is spread between them. We have obtained an initial value of $P_{C\equiv C} \approx 2$, confirming the delocalization of the initial excited state between both two-ring PPE units.[63]

We will now investigate the mechanism that leads to the highly efficient ultrafast intramolecular energy transfer by exploring the role of the nuclear differential motion on the different potential energy surfaces. Figure 6 displays histograms of the energy gap $\Delta E_{i,i-1}^{\text{X-ring}}$ between the $S_i$ and $S_{i-1}$ states (solid lines) and the energy gap $\Delta E_{i+1,i}^{\text{X-ring}}$ between the $S_{i+1}$ and $S_i$ states (dashed lines) while nuclei are moving on the *ith* state whose transition density is more than 90% localized on the X-ring linear PPE unit (X = 2,3, and 4). First, relatively small values of $\Delta E_{i,i-1}^{\text{2-ring}}$ indicate that the nuclear motion on electronic excited states whose transition densities are localized on the two-ring units keeps the current $i$ state close to the one immediately below it. According to the Hellmann-Feynman theorem,[47] this feature favours the energy transfer between them since the nonadiabatic cou-

plings $\mathbf{d}_{i,(i-1)}$ are proportional to $1/\Delta E_{(i-1)\text{-}i}$. On the other hand, large value of $\Delta E_{i+1,i}^{\text{3-ring}}$ indicates that while the system transfers its electronic population to surfaces whose transition densities are localized on the three-ring unit, the energy gaps between these states increase, separating the surfaces. Therefore, $\Delta E_{i,i-1}^{\text{2-ring}} < \Delta E_{i+1,i}^{\text{3-ring}}$ guarantees the unidirectional two-ring→three-ring energy transfer. Thereafter, while the excitation energy remains localized in the three-ring unit, we observe that $\Delta E_{i,i-1}^{\text{3-ring}} < \Delta E_{i+1,i}^{\text{3-ring}}$. While the current state $i$ is localized in the three-ring unit, the $i+1$ state is likely to be in the two-ring unit while the $i$-1 state is in the four-ring unit. Therefore, $\Delta E_{i,i-1}^{\text{3-ring}} < \Delta E_{i+1,i}^{\text{3-ring}}$ indicates that the three-ring →four-ring energy transfer will be more likely than the three-ring→two-ring one. Finally, $\Delta E_{i,i-1}^{\text{3-ring}} < \Delta E_{i+1,i}^{\text{4-ring}}$ ensures that the energy flow in the opposite direction four-ring → three-ring is negligible. In summary, the fact that $\Delta E_{i,i-1}^{\text{X-ring}} < \Delta E_{i+1,i}^{(X+1)\text{-ring}}$ guarantees an efficient unidirectional two-ring → three-ring→four-ring energy flow within the model dentritic molecule. It is important to stress that this analysis have been preformed considering our simplified *coarse grained* description of the process in terms of the time-dependent localization of the transition density of states. Obtained results are consistent with previous data obtained in terms of specific adiabatic excited electronic states.[58] Figure 7 outlines what we call the *Shishiodoshi unidirectional energy transfer mechanism* due to its similarity to the well-known mechanism of a Japanese bamboo water fountain. That is, while the electronic population is mostly on states with transition densities localized in the two-ring units, the energy gap between the current state and the state immediately below remains small. Therefore, the energy flows between them. Once the electronic population has been substantially transferred to states localized on the three-ring unit, the nuclear motion on the new surface decouples these states but starts to couple the new state with the corresponding state immediately below. The energy transfer between these new states persists until most of the population has been transferred to the state localized in the four-ring unit. After that, these latter states then separate from each other.

As we have shown previously[18,58] the intramolecular vibrational energy redistribution that accompanies the electronic energy transfer can be followed by analyzing the time
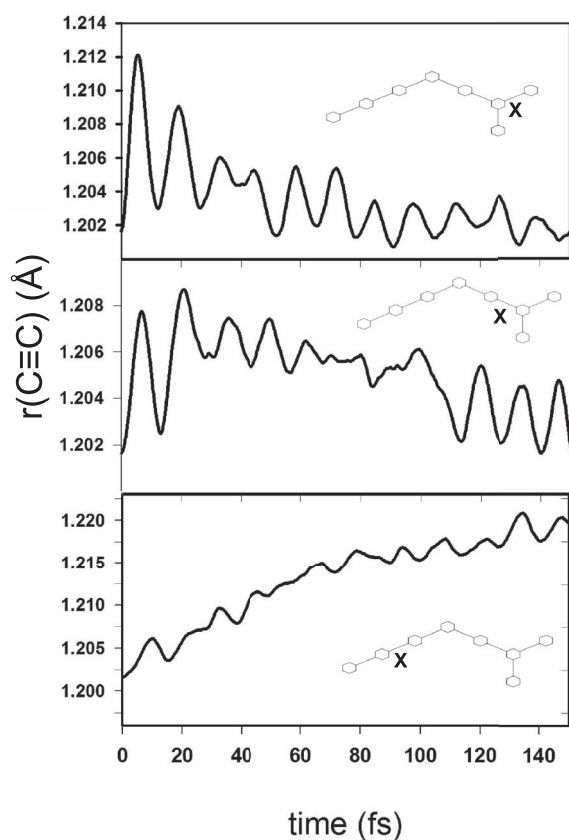
FIG. 8. Length of particular ethynylene bonds (labeled X) as a function of time obtained from the average of trajectories that reach final states with transition densities 90% localized in the 4-ring linear PE unit.



FIG. 9. Histograms for lengths of the ethynylene bonds while nuclei are moving on states whose transition densities are more than 90% (solid lines) or less than 10% (dashed lines) localized in the X-ring linear PE unit (X = 2, 3, and 4 for (a), (b), and (c), respectively).

evolution of the average over all trajectories of the ethynylene bond lengths (Figure 8). The stretching of the triple bonds of the two-ring components becomes highly excited immediately after the initial vertical electronic excitation of the molecule. This initially localized excess of vibrational energy is rapidly dampened while nonradiative transitions from the initial electronic excited state to other electronic excited states localized in the three- and four-ring units take place. The stretching of the triple bonds of the three-ring unit, while partially vibrational excited due to direct initial electronic excitation to states localized in the three-ring unit, act as intermediates in the vibrational energy flow throughout the molecule. Finally, the stretching of the triple bonds of the four-ring unit gets progressively larger in time reaching a maximum at the end of the NA-ESMD simulations. At this point it is interesting to stress that the coherent vibrational motion observed during the first oscillations of the ethynylene bond corresponds to a coherence associated to the classical motion of the ethynylene bonds as harmonic oscillator, as has been recently pointed out by W. H. Miller.[66] Likely a quantum treatment of these high frequency motions will average out, at least partially, these coherent dynamics.

Finally, we analyze the concurrence of the electronic and vibrational excitations. Figure 9 shows histograms for lengths of the ethynylene bonds while nuclei are moving on states whose transition densities are more than 90% (solid lines) or less than 10% (dashed lines) localized in the X-ring linear
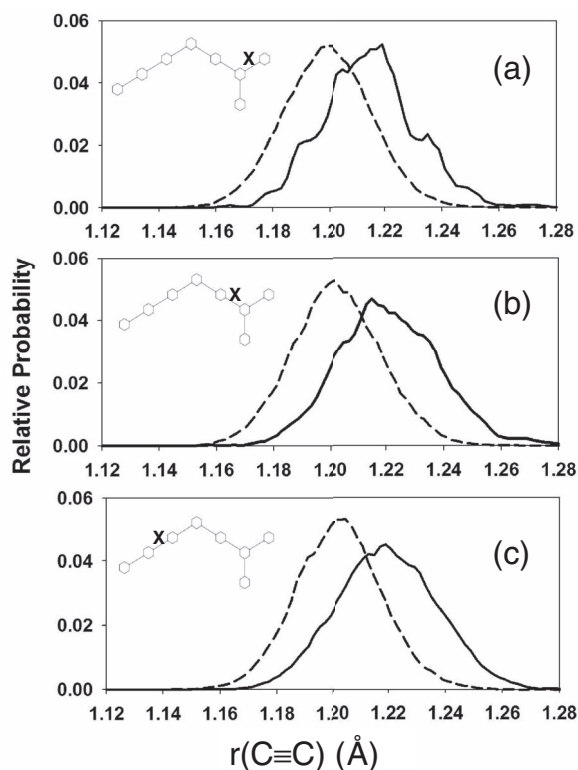
PPE unit (X = 2, 3, and 4 for (a), (b), and (c) respectively). As can be seen, the localization of triple bond excitations coincides with the localization of the electronic transition densities. Therefore, the photoinduced dynamics can be defined as a concerted unidirectional electronic and vibrational energy transfer process.

## IV. CONCLUSIONS

We have performed non-adiabatic excited state molecular dynamics simulations of a polyphenylene ethynylene dendrimer composed of meta-linked two-, three-, and four-ring linear PPE units. Simulations were done using the well-studied Tully's fewest switches surface hopping algorithm and a recently developed state reassignment algorithm has been implemented to treat regions of unavoided state crossings. Our analysis reveals the microscopic determinants for concerted unidirectional electronic and vibrational energy transfer between the PPE units.

We have shown that the unidirectional energy transfer process cannot be easily expressed in terms of the evolution of the populations on each adiabatic electronic excited state given by energy ordering. This is due to the multiple crossings and mixing that the states undergo over time. Therefore, we have proposed a novel alternative based on following the changes in the localization of the electronic transition density of the current state. In this way we have observed that the initial excitation is localized on the two-ring units and that the energy transfer to the three- and four-ring units is

complete within $\sim 80$–100 fs as the transition density gradually becomes localized in the four-ring unit. Further investigation of the changes in the localization of the electronic transition densities revealed that the energy transfer occurs via both through-space and through-bond pathways.

The initial state is always spread between both of the two-ring units with some delocalization between the two- and three-ring units as indicated by the triple bond participation number. Our results confirm that the highly efficient ultrafast intramolecular energy transfer is unidirectional proceeding sequentially via two-ring→three-ring→four-ring energy flow within the model dentritic molecule. The energy gaps between the excited states are coupled to the nuclear motions resulting in a *Shishiodoshi*-like energy transfer where, once the electronic population has been transferred to the state directly below in energy, the two states decouple thereby preventing energy transfer in the opposite direction.

Finally, we are able to relate the transfer of electronic energy from the two- to three- to four-ring PPE units with a coinciding vibrational energy transfer by examining the stretching motions in the direction of the ethynylene bonds. As expected, the excitation of the ethynylene triple bond accompanies the localization of the electronic transition density indicating that the triple bond stretching motion is required for the energy transfer to proceed. The efficient two-ring→three-ring→four-ring vibrational energy transfer accompanies the electronic energy transfer and is also unidirectional.

## ACKNOWLEDGMENTS

[1] K. M. Coakley and M. D. McGehee, Chem. Mater. **16**, 4533 (2004).
[2] R. H. Friend, R. W. Gymer, A. B. Holmes, J. H. Burroughes, R. N. Marks, C. Taliani, D. D. C. Bradley, D. A. dos Santos, J. L. Bredas, M. Logdlund, and W. R. Salaneck, Nature (London) **397**, 121 (1999).
[3] R. H. Friend, Pure Appl. Chem. **73**, 425 (2001).
[4] M. A. Baldo, M. E. Thompson, and S. R. Forrest, Nature (London) **403**, 750 (2000).
[5] J. L. Bredas, J. E. Norton, J. Cornil, and V. Coropceanu, Acc. Chem. Res. **42**, 1691 (2009).
[6] D. G. Kuroda, C. P. Singh, Z. Peng, and V. D. Kleiman, Science **326**, 263 (2009).
[7] S. Mukamel, Nature (London) **388**, 425 (1997).
[8] J. M. J. Fréchet, Science **263**, 1710 (1994).
[9] S. F. Swallen, Z. Zhu, J. S. Moore, and R. Kopelman, J. Phys. Chem. B **104**, 3988 (2000).
[10] D. Rana and G. Gangopadhyay, Chem. Phys. Lett. **334**, 314 (2001).
[11] Z. Xu, M. Kahr, K. L. Walker, C. L. Wilkins, and J. S. Moore, J. Am. Chem. Soc. **116**, 4537 (1994).
[12] C. Wu, S. V. Malinin, S. Tretiak, and V. Y. Chernyak, Nat. Phys. **2**, 631, (2006).
[13] R. Kopelman, M. Shortreed, Z. Y. Shi, W. Tan, Z. Xu, J. S. Moore, A. Bar-Haim, and J. Klafter, Phys. Rev. Lett. **78**, 1239 (1997).
[14] W. Chao, S. V. Malinin, S. Tretiak, and V. Chernyak, Nat. Phys. **2**, 631 (2006).
[15] S. F. Swallen, R. Kopelman, J. S. Moore, and C. Devadoss, J. Mol. Struct. **485**, 585 (1999).
[16] C. Devadoss, P. Bharathi, and J. S. Moore, J. Am. Chem. Soc. **118**, 9635 (1996).
[17] M. R. Shortreed, S. F. Swallen, Z. Y. Shi, W. Tan, Z. Xu, C. Devadoss, J. S. Moore, and R. Kopelman, J. Phys. Chem. B **101**, 6318 (1997).
[18] S. Fernandez-Alberti, V. D. Kleiman, S. Tretiak, and A. E. Roitberg, J. Phys. Chem. A **113**, 7535 (2009).
[19] O. V. Prezhdo, W. R. Duncan, and V. V. Prezhdo, Prog. Surf. Sci. **84**, 30 (2009).
[20] C. F. Craig, W. R. Duncan, and O. V. Prezhdo, Phys. Rev. Lett. **95**, 163001 (2005).
[21] W. R. Duncan and O. V. Prezhdo, Annu. Rev. Phys. Chem. **58**, 143 (2007).
[22] B. F. Habenicht and O. V. Prezhdo, Nat. Nanotechnol. **3**, 190 (2008).
[23] E. R. Dunkel, S. Bonella, and D. F. Coker, J. Chem. Phys. **129**, 114106 (2008).
[24] P. Huo and D. F. Coker, J. Chem. Phys. **133**, 184108 (2010).
[25] J. C. Tully, J. Chem. Phys. **93**, 1061 (1990).
[26] I. Antol, M. Eckert-Maksic, M. Barbatti, and H. Lischka, J. Chem. Phys. **127**, 234302 (2007).
[27] G. Zechmann, M. Barbatti, H. Lischka, J. Pittner, and V. Bonačić-Koutecký, Chem. Phys. Lett. **418**, 377 (2006).
[28] M. Barbatti, G. Granucci, M. Persico, and H. Lischka, Chem. Phys. Lett. **410**, 276 (2005); M. Barbatti, M. Ruckenbauer, and H. Lischka, J. Chem. Phys. **122**, 17307 (2005).
[29] M. Pederzoli, J. Pittner, M. Barbatti, and H. Lischka, J. Phys. Chem. A **115**, 11136 (2011).
[30] M. Ruckenbauer, M. Barbatti, B. Sellner, T. Muller, and H. Lischka, J. Phys. Chem. A **114**, 12585 (2010).
[31] M. Barbatti, M. Vazdar, A. J. A. Aquino, M. Eckert-Maksić, and H. Lischka, J. Chem. Phys. **125**, 164323 (2006).
[32] J. Clark, T. Nelson, S. Tretiak, G. Cirmi, and G. Lanzani, Nat. Phys. **8**, 225 (2012).
[33] C. Devadoss, P. Bharathi, and J. S. Moore, J. Am. Chem. Soc. **118**, 9635 (1996).
[34] Z. Xu, M. Kahr, K. L. Walker, C. L. Wilkins, and J. S. Moore, J. Am. Chem. Soc. **116**, 4537 (1994).
[35] S. Fernandez-Alberti, A. E. Roitberg, T. Nelson, and S. Tretiak, J. Chem. Phys. **137**, 014512 (2012).
[36] T. Nelson, S. Fernandez-Alberti, V. Chernyak, A. E. Roitberg, and S. Tretiak, J. Phys. Chem. B **115**, 5402 (2011).
[37] S. Tretiak, A. Saxena, R. L. Martin, and A. R. Bishop, Phys. Rev. Lett. **89**, 097402 (2002).
[38] S. Tretiak, A. Saxena, R. L. Martin, and A. R. Bishop, Proc. Natl. Acad. Sci. U.S.A. **100**, 2185 (2003).
[39] G. A. Worth, M. A. Robb, and B. Lasorne, Mol. Phys. **106**, 2077 (2008).
[40] S. Hammes-Schiffer and J. C. Tully, J. Chem. Phys. **101**, 4657 (1994).
[41] J. C. Tully, "Nonadiabatic molecular dynamics," Int. J. Quantum Chem. **40**, 299 (1991).
[42] S. Tretiak and S. Mukamel, Chem. Rev. **102**, 3171 (2002).
[43] V. Chernyak, M. F. Schulz, S. Mukamel, S. Tretiak, and E. V. Tsiper, J. Chem. Phys. **113**, 36 (2000).
[44] S. Tretiak, C. Isborn, A. Niklasson, and M. Challacombe, J. Chem. Phys. **130**, 054111 (2009).
[45] F. Furche and R. Ahlrichs, J. Chem. Phys. **117**, 7433 (2002).
[46] S. Tretiak and V. Chernyak, J. Chem. Phys. **119**, 8809 (2003).
[47] M. Tommasini, V. Chernyak, and S. Mukamel, Int. J. Quantum Chem. **85**, 225 (2001).
[48] V. Chernyak and S. Mukamel, J. Chem. Phys. **112**, 3572 (2000).
[49] R. Send and F. Furche, J. Chem. Phys. **132**, 044107 (2010).
[50] S. Mukamel, S. Tretiak, T. Wagersreiter, and V. Chernyak, Science. **277**, 781 (1997).
[51] S. Tretiak, V. Chernyak, and S. Mukamel, J. Chem. Phys. **105**, 8914 (1996).
[52] S. Tretiak, W. M. Zhang, V. Chernyak, and S. Mukamel, Proc. Nat. Acad. Sci. U.S.A. **96**, 13003 (1999).
[53] M. J. S. Dewar, E. G. Zoebisch, E. F. Healy, and J. J. P. Stewart, J. Am. Chem. Soc. **107**, 3902 (1985).
[54] T. Nelson, S. Fernandez-Alberti, V. Chernyak, A. E. Roitberg, and S. Tretiak, J. Chem. Phys. **136**, 054106 (2012).
[55] S. Tretiak, V. Chernyak, and S. Mukamel, J. Am. Chem. Soc. **119**, 11408 (1997).

[56]S. Tretiak, V. Chernyak, and S. Mukamel, Chem. Phys. Lett. **259**, 55 (1996).

[57]M. G. Paterlini and D. M. Ferguson, Chem. Phys. **236**, 243 (1998).

[58]S. Fernandez-Alberti, V. D. Kleiman, S. Tretiak, and A. E. Roitberg, J. Phys. Chem. Lett. **1**, 2699 (2010).

[59]H. Hirai and O. Sugino, Phys. Chem. Chem. Phys. **11**, 4570 (2009).

[60]L. Verlet, Phys. Rev. **159**, 98 (1967).

[61]T. Tada, D. Nozaki, M. Kondo, and K. Yoshizawa, J. Phys. Chem. B **107**, 14204 (2003).

[62]J. L. Palma, E. Atas, L. Harrison, T. B. Marder, J. C. Collings, A. Beeby, J. S. Melinger, V. D. Kleiman, J. L. Krause, and A. E. Roitberg, J. Chem. Phys. C **114**, 20702 (2010).

[63]See supplementary material at http://dx.doi.org/10.1063/1.4745835 for the distribution of the initial transition densities between the two-ring linear PE units and the time evolution of PC≡C.

[64]R. J. Bell, P. Dean, and C. Hibbins-Butler, J Phys C: Solid State Phys. **3**, 2111 (1970).

[65]S. N. Taraskin and S. R. Elliott, Phys Rev B **59**, 8572 (1999).

[66]W. H. Miller, J. Chem. Phys. **136**, 210901 (2012).